

## Corrosion Behavior of Mo<sub>5</sub>Si<sub>3</sub>-Based Metal Silicide Alloy

H. Chen<sup>1,\*</sup>, Q. Ma<sup>2</sup>, X. Shao<sup>1</sup>, J. Ma<sup>1</sup>, B. X. Huang<sup>1</sup>

<sup>1</sup> College of Materials Science and Engineering, Liaocheng Research Institute of Non-ferrous Metals, Liaocheng University, Liaocheng 252000, China

<sup>2</sup> State Key Laboratory of Gansu Advanced Non-ferrous Metal Materials, School of Materials Science and Engineering, Lanzhou University of Technology, Lanzhou 730050, China

\*E-mail: [chenhui002@qq.com](mailto:chenhui002@qq.com)

Received: 26 October 2012 / Accepted: 18 November 2012 / Published: 1 December 2012

---

The Mo<sub>5</sub>Si<sub>3</sub>-based alloy consisting of small particles Mo<sub>3</sub>Si uniformly distributed in a Mo<sub>5</sub>Si<sub>3</sub> matrix was fabricated by hot press sintering method. Corrosion properties of the alloy were investigated using anodic polarization and immersion tests in 1 mol/L HCl, 1 mol/L H<sub>2</sub>SO<sub>4</sub> and 1 mol/L NaOH solutions, respectively. Results showed that the alloy had very low corrosion rate in three tests solutions due to the formation of a stable and compact passive film (SiO<sub>x</sub>, MoO<sub>3</sub> and MoO<sub>2</sub>) as well as the chemical stability and strong bonds with large covalent component inherent to Mo<sub>5</sub>Si<sub>3</sub>-based alloy. Only a slight pitting could be observed on the sample surface as a result of selective corrosion of the Mo<sub>3</sub>Si phases with respect to the Mo<sub>5</sub>Si<sub>3</sub> matrix in NaOH solution. Meanwhile, the alloy exhibited excellent electrochemical corrosion resistance in acidic environments excluding NaOH solution. The alloy was less corrosion resistance because of the formation and dissolution of Na<sub>2</sub>SiO<sub>3</sub> and damaging the integrity of SiO<sub>2</sub> preservative in NaOH solution.

---

**Keywords:** Metal silicide; Corrosion; Mo<sub>5</sub>Si<sub>3</sub>; Passive film; Intermetallics

### 1. INTRODUCTION

In recent days, there is a need for materials with good properties to support extreme conditions such as high-temperature, high stresses and corrosive environments [1]. Wear and corrosion are two of the three most frequently encountered failure modes for mechanical components working under aggressive service conditions [2,3]. Many industries components are more severely degraded by the interaction of wear and corrosion. However, traditional materials are not always able to meet both the corrosion and wear resistance simultaneously [4,5]. Therefore, development of new materials working in corrosion and wear environments has important significance [6].

Mo-Si refractory metal silicides have many attractive properties such as high melting point, high hardness and excellent chemical stability due to their strong atomic bonds [7-11]. D8m-structured  $\text{Mo}_5\text{Si}_3$  is the most refractory compound in the Mo-Si binary system with a melting point of 2180 °C [12,13]. And it has a great potential for structural application in harsh environment. It is well known that their high-temperature oxidation stability is due to the formation of a highly protective  $\text{SiO}_2$  layer [14-16]. Meanwhile, due to its high hardness, unique chemical composition and strong bonds with large covalent component,  $\text{Mo}_5\text{Si}_3$  is anticipated to be a novel wear and corrosion resistant candidate material [17]. While many studies for the strengthening and toughening of  $\text{Mo}_5\text{Si}_3$  have been reported, corrosion behaviors of  $\text{Mo}_5\text{Si}_3$  have hardly attempted [11,18].

Microstructural characteristics and compactness are considered to be beneficial to increase the corrosion resistance [11]. However, due to their high melting point and high vapour pressure, the complete densification of pure Mo and Si powder mixtures needs extremely high sintering temperatures.  $\text{Mo}_5\text{Si}_3$  alloys have been synthesized by various methods such as arc-melting and casting, mechanical alloying, solid-state displacement reaction and self-propagating high-temperature synthesis [19-21]. However, the limitation of all these methods lies in that they are time consuming, microstructure stress and defects or the products are porous. Compared with those techniques mentioned above, medium frequency induction hot-pressing method has a high-energy heat source for sintering simultaneously with a uniaxial pressure to primarily sinter powders. This method ensures a very rapid heating rate and mass transfer speed, and allows the sample to be fabricated in a short period time at a relatively lower temperature. Some silicides and ceramics prepared by hot-pressing sintering have a high density and fine microstructure.

In this study, corrosion behaviors of a hot pressing sintered  $\text{Mo}_5\text{Si}_3$  were investigated in 1 mol/L HCl, 1 mol/L  $\text{H}_2\text{SO}_4$  and 1 mol/L NaOH solutions. Anodic potentiodynamic polarization and immersion tests were performed to evaluate the corrosion resistance of the  $\text{Mo}_5\text{Si}_3$ -based alloy. The corrosion properties of  $\text{Mo}_5\text{Si}_3$ -based alloy and corresponding corrosion mechanisms were studied in details.

## 2. EXPERIMENTAL

Commercial pure molybdenum and silicon elemental powders in purity of 99.5% and an average particle size ranging from 3 to 5  $\mu\text{m}$  were selected as the raw materials. The powders were blended and milled in a planetary ball mill at room temperature. Ball-to-powder weight ratio was 10:1 and rotation speed 300 rpm. The milled powder was loaded into a cylindrical carbon die with an inner diameter of 25 mm. The sintering temperature was set to 1450 °C (the melting point of silicon is 1415 °C and liquid phase sintering is promising for higher density) and the sample was heated at a rate of 75 K/min and kept at 1450 °C for 30 min. Meanwhile, a uniaxial pressure of 50 MPa was applied during the sintering cycle. The hot pressed product was a plate of 25 mm diameter and approximately 8mm thickness. Microstructure of  $\text{Mo}_5\text{Si}_3$  alloy was characterized by JSM-6700F scanning electron microscopy (SEM). Phases of the alloy were determined by X-ray diffraction using the Rigaku D/max-2400 pc automatic X-ray diffractometer with Cu target  $\text{K}\alpha$  radiation ( $\lambda=0.15418$  nm). Chemical

compositions of the phase constituents were analyzed by energy dispersive X-ray analysis (EDS). The relative density of the alloy was measured by the Archimedes method.

Corrosion testing specimens were electrical discharge machined into 8 mm×8 mm×6 mm. Prior to the electrochemical tests, the specimens were ground up to 2000 grit SiC emery paper. Then, they were ultrasonically cleaned in acetone and kept in desiccators for 10 h. Corrosion resistance of alloy was investigated by immersion and anodic potentiodynamic polarization measurements at ambient temperature ( $\sim 25\text{ }^{\circ}\text{C}$ ) in 1 mol/L HCl, 1 mol/L  $\text{H}_2\text{SO}_4$  and 1 mol/L NaOH solutions, respectively. The corrosion solutions were prepared from reagent grade chemical and distilled water. Electrochemical measurements (CH1604C instrument) were conducted in a three-electrode cell, using a platinum counter electrode and a saturated calomel reference electrode. Experiments were performed by sweeping potential from -1000 to 2000 mV at a scan rate of 2 mV/s. All the tests were repeated at least three times for accuracy.

Austenitic stainless steel 0Cr18Ni9 was selected as the reference materials for both immersion and anodic polarization tests. The surface of samples after experiments was investigated using scanning electron microscopy. Meanwhile, in order to obtain a stable passive film for X-ray photoelectron spectrometer analysis using the AXIS Ultra X-ray photoelectron spectrometer with Al  $\text{K}\alpha$  (1486.71 eV) monochromatic radiation, the electrochemical constant-potential passivation treatment at applied potential of 0.1 V for 10 min was conducted for the  $\text{Mo}_5\text{Si}_3$  alloy in 1 mol/L HCl solution. Peak identification was performed by reference to a XPS database.

Immersion corrosion tests were conducted by immersing the  $\text{Mo}_5\text{Si}_3$  alloy in 1 mol/L HCl, 1 mol/L  $\text{H}_2\text{SO}_4$  and 1 mol/L NaOH water solutions at ambient temperature for 100 h. The immersion corrosion resistance of the  $\text{Mo}_5\text{Si}_3$  alloy and 0Cr18Ni9 was characterized by measuring the corrosion induced mass loss using a precision electronic balance with an accuracy of 0.1 mg. Corrosion rates were estimated from mass loss after immersion in these solutions.

### 3. RESULTS

#### 3.1 Microstructure

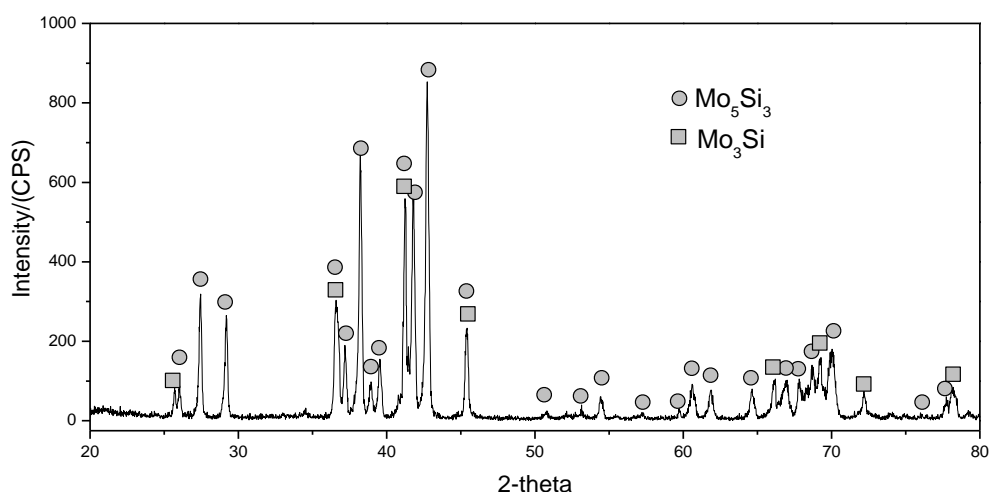


**Figure 1.** X-ray diffraction pattern of the  $\text{Mo}_5\text{Si}_3$  alloy

As shown in Fig. 1, the XRD pattern of the sample shows the main phase constituents of the alloy are  $\text{Mo}_5\text{Si}_3$  and a small amount of  $\text{Mo}_3\text{Si}$ . As shown in Fig. 2, the  $\text{Mo}_5\text{Si}_3$  alloy has a uniform microstructure free from pores and micro-cracks.

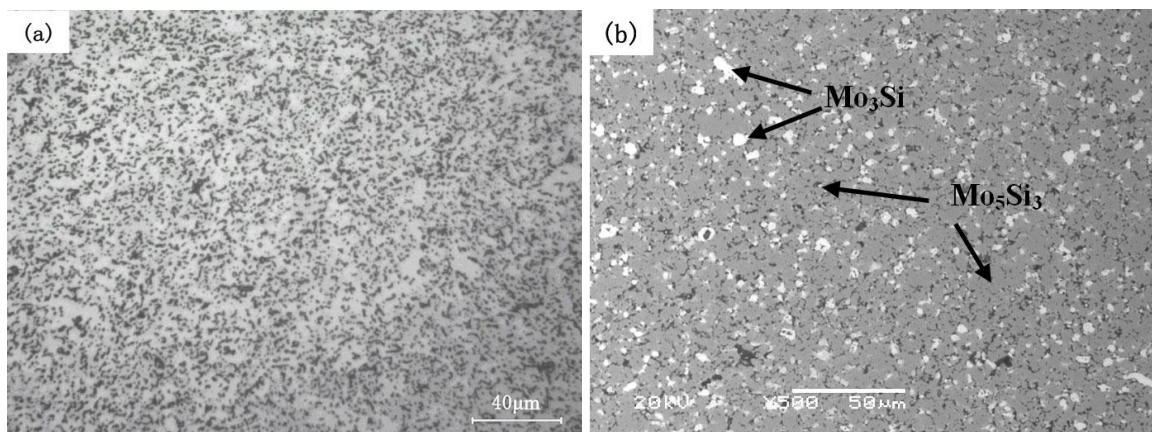


**Figure 2.** OM (a) and SEM (b) micrographs showing microstructure of the  $\text{Mo}_5\text{Si}_3$  metal silicide alloy

### 3.2 Electrochemical test

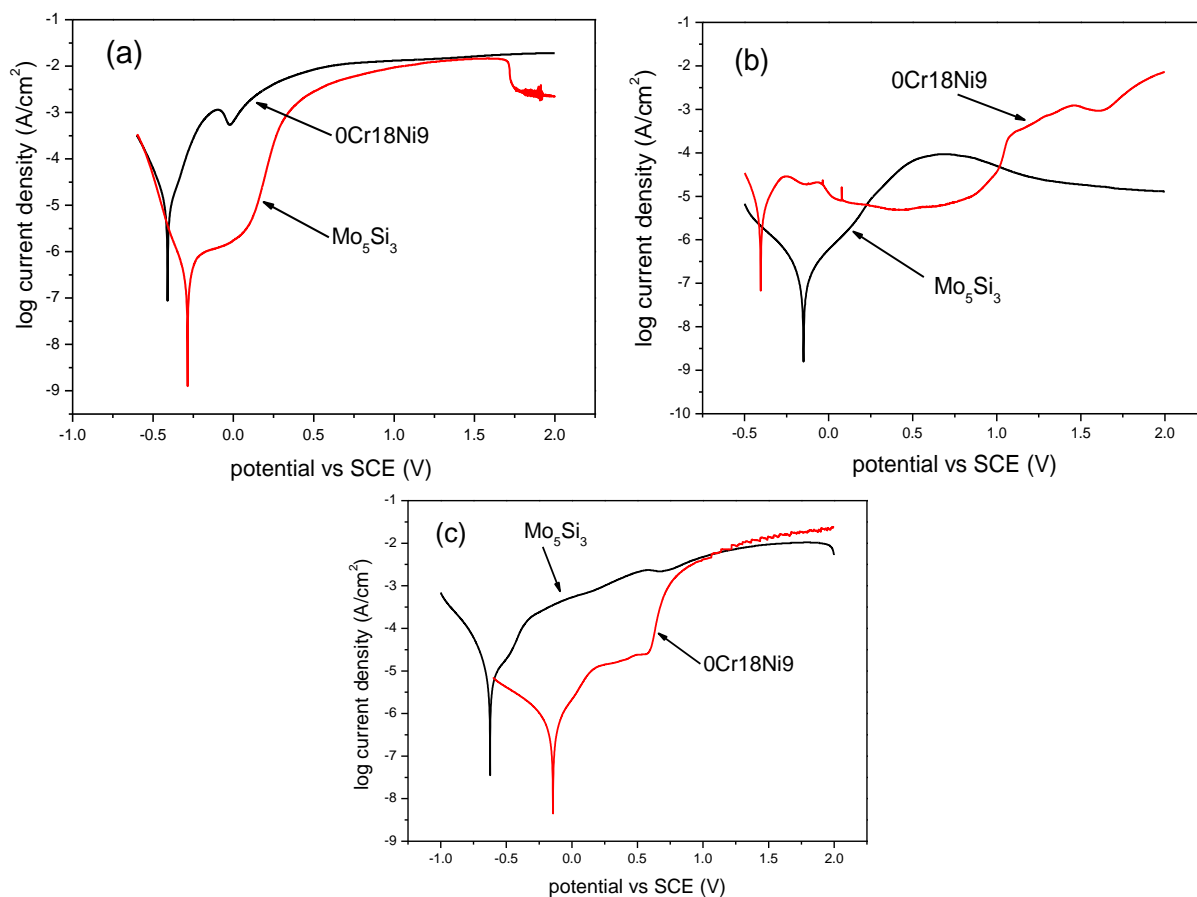


**Figure 3.** Anodic potentiodynamic polarization curves of the  $\text{Mo}_5\text{Si}_3$  alloy in comparison to the stainless steel 0Cr18Ni9 in 1 mol/L HCl (a), 1 mol/L  $\text{H}_2\text{SO}_4$  (b) and 1 mol/L NaOH (c) solutions

The relative density of sample is 97.3%. The specimen contains small particles  $\text{Mo}_3\text{Si}$  uniformly distributed in a  $\text{Mo}_5\text{Si}_3$  matrix. Result of EDS analysis (gray phase: 62.24Mo-37.76Si, at.% and white phase: 71.49Mo-28.51Si, at.%) demonstrate that the gray matrix is the  $\text{Mo}_5\text{Si}_3$  phase and the white phase is  $\text{Mo}_3\text{Si}$ . Volume fraction of  $\text{Mo}_5\text{Si}_3$  phase and  $\text{Mo}_3\text{Si}$  phase are approximately 83% and 17%, respectively.

Fig. 3(a) shows the polarization curves of the  $\text{Mo}_5\text{Si}_3$  alloy and austenitic stainless steel 0Cr18Ni9 in 1 mol/L HCl water solution at room-temperature. When the potential is anodically scanned, no active-passive transition range was observed on the anodic polarization curves of  $\text{Mo}_5\text{Si}_3$  alloy, indicating that the alloy is passivated immediately. The anodic current density of the alloy increases gradually after a short passivation range on the anodic polarization curve, suggesting transpassive dissolution of the alloy. At higher potential, the anodic current density of the alloy decreases obviously with the increasing potential as a result of secondary passivation of the alloy. The  $\text{Mo}_5\text{Si}_3$  alloy has higher corrosion potential and much lower corrosion current density compared with the 0Cr18Ni9 stainless steel, implying that the  $\text{Mo}_5\text{Si}_3$  alloy exhibited excellent corrosion resistance than the 0Cr18Ni9 stainless steel in 1mol/L HCl solution.

As shown in Fig. 3(b), the potentiodynamic anodic polarization curves of the  $\text{Mo}_5\text{Si}_3$  alloy in 1 mol/L  $\text{H}_2\text{SO}_4$  solution has the similar shape with that of the alloy in 1 mol/L HCl solution. Although the austenitic stainless steel has a wide passivation region, the present alloy has considerably higher corrosion potential and much lower corrosion current density compared with the stainless steel 0Cr18Ni9, showing that the  $\text{Mo}_5\text{Si}_3$ -based alloy exhibits high corrosion resistance in 1 mol/L  $\text{H}_2\text{SO}_4$  solution.

As indicated in Fig. 3(c), the  $\text{Mo}_5\text{Si}_3$  alloy has a lower corrosion potential and a higher current density than 0Cr18Ni9 at the initial stage. Meanwhile, the corrosion potential of the alloy in 1 mol/L NaOH solution is obviously negative than that in the other two solutions, which also indicates the relatively high susceptibility of the alloy to electrochemical corrosion in alkaline medium.

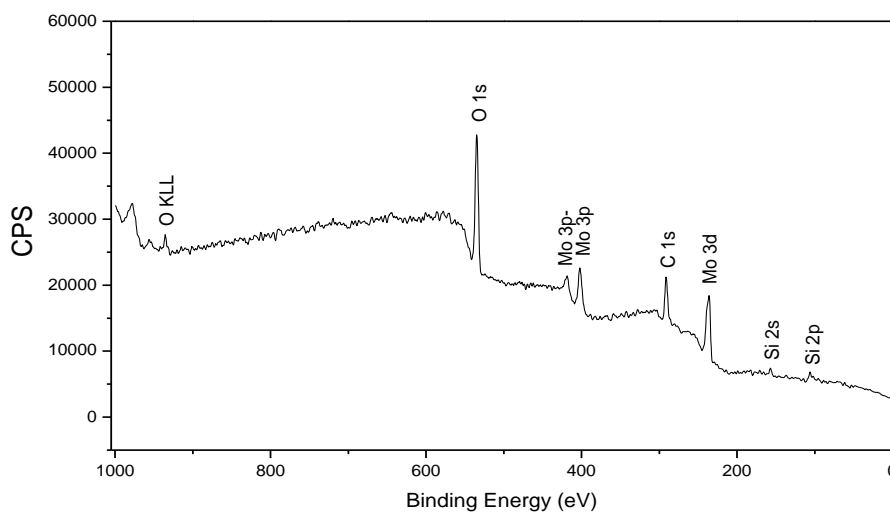


**Figure 4.** XPS survey spectra of the  $\text{Mo}_5\text{Si}_3$ -based alloy after passivation at 0.1 V vs. SCE for 10 min in 1 mol/L HCl solution

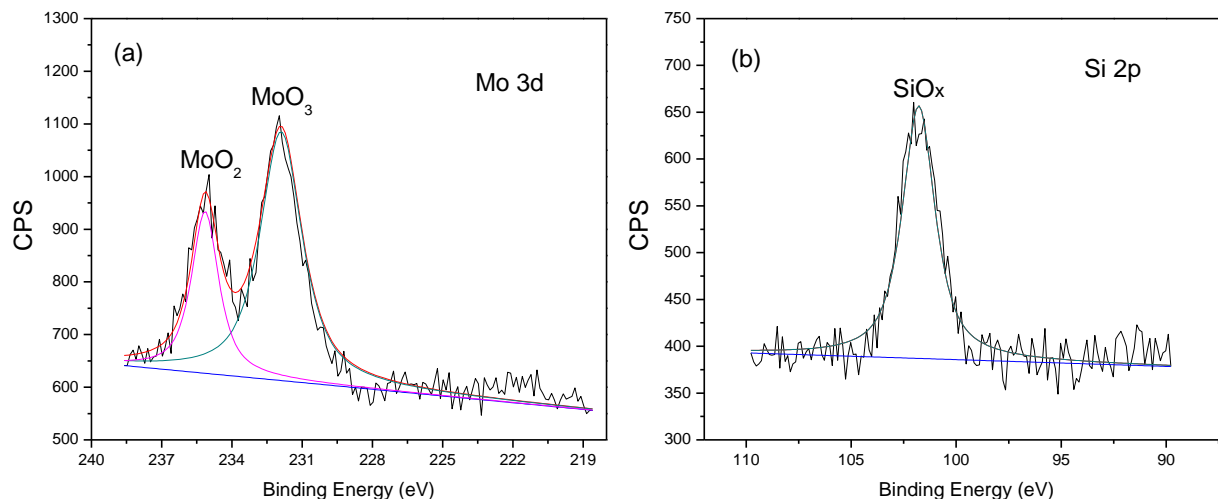


**Figure 5.** High-resolution XPS spectra of Mo<sub>5</sub>Si<sub>3</sub>-based alloy after 10 min potentiostatic polarization at 0.1 V vs. SCE in 1 mol/L HCl solution: (a) Mo 3d, (b) Si 2p

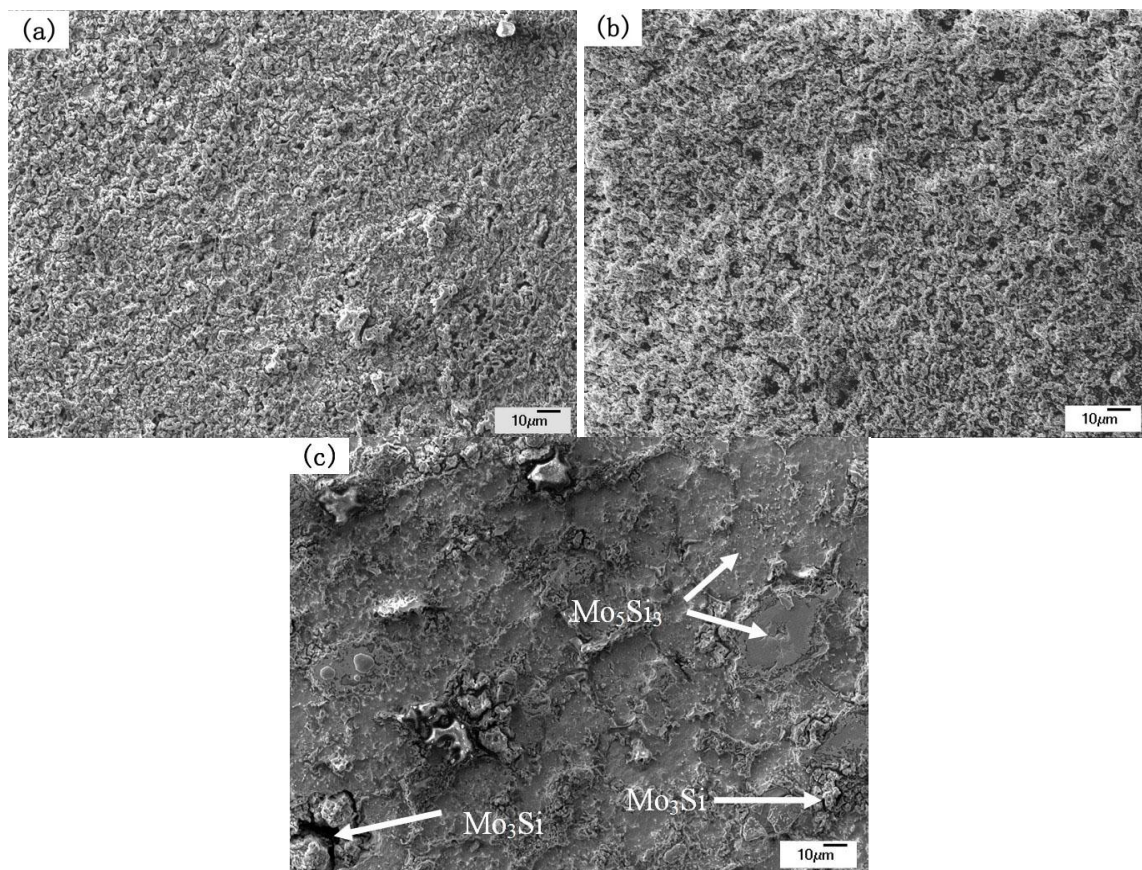


**Figure 6.** Surface morphologies of the Mo<sub>5</sub>Si<sub>3</sub> alloy after anodic potentiodynamic polarization in 1 mol/L HCl(a), 1 mol/L H<sub>2</sub>SO<sub>4</sub>(b) and 1 mol/L NaOH(c).

Corrosion behavior of material is often controlled by the properties of surface passive film. Passive films of Mo<sub>5</sub>Si<sub>3</sub>-based alloy after passivation at 0.1 V vs. SCE in 1 mol/L HCl solution were

studied by XPS (as shown in Fig. 4), exhibit peaks of Mo, Si, O and C. The C 1s peak possibly arose from a contaminant hydrocarbon layer covering the specimen surface [17]. In order to further determine the film components, the high-resolution XPS spectra of Mo 3d and Si 2p regions were recorded, as shown in Fig. 5. The Mo 3d spectrum consist of two peaks at 231.79 eV and 235.1 eV, which are designated as MoO<sub>3</sub> and MoO<sub>2</sub>, respectively. The Si 2p spectrum with a binding energy of 101.8 eV, corresponded to Si in silicon oxides form (SiO<sub>x</sub>). This is close to the results obtained by Jiang [11], who reported that Si 2p peak was made up of oxidized components (SiO<sub>x</sub>) in the passive film on the (Mo<sub>x</sub>Cr<sub>1-x</sub>)<sub>5</sub>Si<sub>3</sub> films in NaCl solution. According to the XPS analysis showed that the main component in the passive film is silicon oxide (SiO<sub>x</sub>) coexisting with molybdenum oxide (MoO<sub>3</sub> and MoO<sub>2</sub>) in HCl solution.

Fig. 6 shows the corrosion surface morphologies of Mo<sub>5</sub>Si<sub>3</sub> alloy after anodic potentiodynamic polarization in three solutions. Compared with Fig. 2(b), it could be observed that the surface of the alloy was obviously destroyed, and become coarse and porous after anodic polarization corrosion in HCl solution, as shown Fig. 6(a). This is mainly attributed to the dissolution of the surface passive film. The surface of the alloy after anodic polarization corrosion in 1mol/L H<sub>2</sub>SO<sub>4</sub> solution has the similar morphology with that of alloy in 1 mol/L HCl solution, as shown Fig. 6(b). However, it is evident from Fig. 6(c) that Mo<sub>5</sub>Si<sub>3</sub>-based alloy has been suffered from the severe attack of OH<sup>-1</sup> ion and a large area of spalling occurs on the corroded surface, and the degree of surface damage dependent on the Si content in Mo<sub>5</sub>Si<sub>3</sub> alloy. In general terms, the phases with lower silicon contents were least corrosion resistant. For instance, as shown in Fig. 6(c) the Mo<sub>3</sub>Si phases were preferentially corroded with respect to the Mo<sub>5</sub>Si<sub>3</sub> matrix. Meanwhile, preferential corroded at the interface of the cluster of grains were found in the case of Mo<sub>5</sub>Si<sub>3</sub> alloy in 1 mol/L NaOH solution.

### 3.3 Immersion corrosion test

The mass loss of the alloy and the stainless steel 0Cr18Ni9 induced by immersion corrosion in the HCl, H<sub>2</sub>SO<sub>4</sub> and NaOH solutions open to air at the room temperature for 100h are shown in Table 1. Meanwhile, the corrosion rates are also calculated according to the mass loss of the alloy and stainless steel. In 1 mol/L HCl and 1 mol/L H<sub>2</sub>SO<sub>4</sub> solutions, stainless steel 0Cr18Ni9 dissolves actively, showing a high corrosion rate of 12.04 mm/a and 12.791 mm/a, respectively. On the other hand, the corrosion rate of Mo<sub>5</sub>Si<sub>3</sub>-based alloy only is 0.064 mm/a and 0.011 mm/a, respectively. Therefore, it is clear that the Mo<sub>5</sub>Si<sub>3</sub>-based alloy has much high corrosion resistance than the reference material in 1mol/L HCl and 1mol/L H<sub>2</sub>SO<sub>4</sub> solutions. In addition, after immersion in HCl, H<sub>2</sub>SO<sub>4</sub> and NaOH solutions for 100 h, the mass loss of alloys is so slight that it could be almost ignored. All the samples maintain good metallic shining after immersion for 100 h in HCl and H<sub>2</sub>SO<sub>4</sub> solutions excluding NaOH solution. As shown in Fig. 7, the surfaces morphologies of alloy specimens and the reference materials are observed by scanning electron microscopy (SEM). No change could be seen on the surface of the alloy after immersion tests in HCl and H<sub>2</sub>SO<sub>4</sub> solutions. Only a slight pitting could be observed on the sample surface after immersion for 100h in NaOH solution. However, the reference material completely loses metallic luster, pitting, ditches and grain boundary corrosion are observed

everywhere throughout the surface after immersion in three solutions for 100h, as shown Fig. 7(b), (d) and (f). Results of mass losses and surface morphologies are consistent and indicate the excellent corrosion resistance of the  $\text{Mo}_5\text{Si}_3$ -based alloy during immersion in the HCl,  $\text{H}_2\text{SO}_4$  and NaOH solutions.

**Table 1.** Results of immersion corrosion tests of the  $\text{Mo}_5\text{Si}_3$ -based alloy and austenitic stainless steel 0Cr18Ni9 in 1 mol/L HCl, 1 mol/L  $\text{H}_2\text{SO}_4$  and 1 mol/L NaOH solutions for 100 h.

Electrolytes	Test materials	Corrosion mass loss(mg)	Corrosion rate (mm)/year
1 mol/L HCl	$\text{Mo}_5\text{Si}_3$ -based alloy	0.6	0.064
	Austenitic stainless steel 0Cr18Ni9	123.4	12.040
1 mol/L $\text{H}_2\text{SO}_4$	$\text{Mo}_5\text{Si}_3$ -based alloy	0.1	0.011
	Austenitic stainless steel 0Cr18Ni9	131.1	12.791
1 mol/L NaOH	$\text{Mo}_5\text{Si}_3$ -based alloy	0.1	0.011
	Austenitic stainless steel 0Cr18Ni9	1.2	0.117

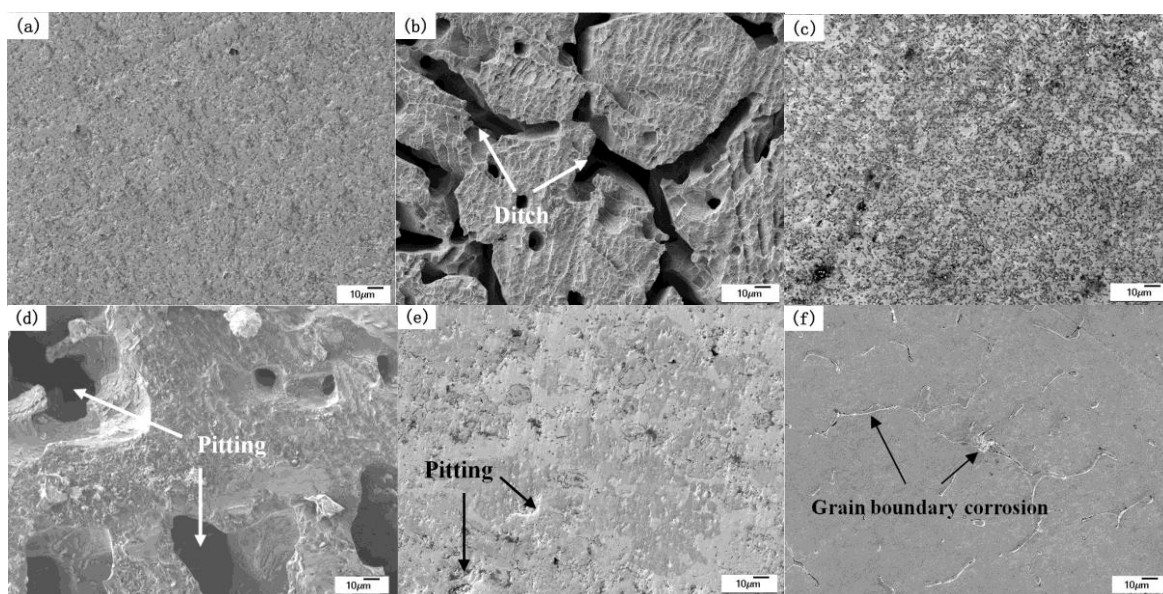


**Figure 7.** SEM images showing the surface morphologies of the  $\text{Mo}_5\text{Si}_3$ -based alloy(a),(c),(e) and austenitic stainless steel(b),(d),(f) after immersion for 100h in 1 mol/L HCl(a),(b), 1 mol/L  $\text{H}_2\text{SO}_4$ (c),(d), and 1 mol/L NaOH solutions(e),(f)

#### 4. DISCUSSIONS

The present experimental results indicated that the  $\text{Mo}_5\text{Si}_3$ -based alloy exhibited excellent corrosion resistance both in the anodic polarization and immersion corrosion tests in HCl and  $\text{H}_2\text{SO}_4$  solutions. In comparison to austenitic stainless steel 0Cr18Ni9 which was widely applied in industries for its outstanding corrosion resistance, the  $\text{Mo}_5\text{Si}_3$ -based alloy was much more corrosion resistance. The considerably higher corrosion potential, much lower corrosion current density and a secondary

passivation region were observed under the anodic polarization test conditions in HCl and H<sub>2</sub>SO<sub>4</sub> solutions. Meanwhile, the alloy displayed relatively low immersion corrosion rates in three solutions. As indicated in Fig. 3(c), though the Mo<sub>5</sub>Si<sub>3</sub> alloy has a lower corrosion potential and a higher current density than 0Cr18Ni9, the mass loss of alloy was much lower in NaOH solution.

As shown in Fig. 7(b), the pits and ditch appeared on the surface of austenitic stainless steel. The micro-pits were gradually connected with each other during the immersion test as a result of the breakdown of the passive film. While, no significant changes were observed on the surface of the Mo<sub>5</sub>Si<sub>3</sub> alloy and the breakdown mechanism of passive film indicating the gradual dissolution mechanism, instead of an abrupt breakdown mechanism of passive film. Two models are used to describe the mechanism of the passive film in HCl solution. For instance, the adsorption of Cl<sup>-</sup> on the passive film and the ion migration or penetration of Cl<sup>-</sup> ion through the passive film to metal surface [6, 22]. While, no signals of chloride ions were detected in the passive film of the Mo<sub>5</sub>Si<sub>3</sub> alloy according to the XPS results. Thus, the absorbed Cl<sup>-</sup> on alloy surface was very low and the passive film was possible formed an p-type semiconductor. It has been found that the p-type film was more insensitive to pitting corrosion than n-type film [23]. Therefore, the Mo<sub>5</sub>Si<sub>3</sub> alloy displayed excellent corrosion resistance in HCl solution.

It is well known that Mo and Si are all strong passive elements in aggressive environments. As indicated by the XPS results in Fig. 4 and Fig. 5, the passive layer formed on the surface of the Mo<sub>5</sub>Si<sub>3</sub>-based alloy is composed mainly of silicon oxide (SiO<sub>x</sub>) and molybdenum oxide (MoO<sub>3</sub> and MoO<sub>2</sub>). The higher molybdenum and silicon contents in this alloy and the high oxygen affinity of molybdenum and silicon would promote the rapid formation of a compact and electrochemically stable oxide passive film on the surface of the alloy, protecting the alloy from further attacks under an aggressive environment was responsible for the high corrosion resistance of the present alloy. Meanwhile, the silicon oxide in the passive film has a significant corrosion inhibition effects, due to its good corrosion resistance and almost insolubility in acidic and neutral media. Furthermore, the chemical stability and strong inter-atomic bonds inherent to Mo<sub>5</sub>Si<sub>3</sub> also make an important contribution to the excellent corrosion-resistance of the Mo<sub>5</sub>Si<sub>3</sub> alloy.

The Mo<sub>5</sub>Si<sub>3</sub> alloy displayed relatively low electrochemical corrosion resistance in 1 mol/L NaOH solution due to the lack of a stable passivation state compared with that in acidic environments. XPS results indicated that the passive film mainly composed of silicon oxide (SiO<sub>2</sub> or SiO). In NaOH solution, SiO<sub>2</sub> reacts with NaOH and formed Na<sub>2</sub>SiO<sub>3</sub> when polarized to a certain anodic potential according to the reaction  $\text{SiO}_2 + \text{OH}^{-1} \rightarrow \text{SiO}^{-3} + \text{H}_2\text{O}$  [17]. Na<sub>2</sub>SiO<sub>3</sub> was dissolved and damaging the integrity of SiO<sub>2</sub> preservative in NaOH solution. In addition, owing to a lack of passive film (SiO<sub>2</sub>), the grain boundary has negative effect on corrosion behavior of the alloy, accelerating corrosion by forming micro-electrochemical cells between grains boundaries and the matrix and by increasing the electrochemical reactivity during the corrosion process, as shown in Fig. 6(c).

## 5. CONCLUSIONS

Mo<sub>5</sub>Si<sub>3</sub>-based alloy was fabricated by hot press sintering with Mo-Si elemental powder blends. Microstructure of Mo<sub>5</sub>Si<sub>3</sub>-based alloy consists of small amount of Mo<sub>3</sub>Si uniformly distributed in a

Mo<sub>5</sub>Si<sub>3</sub> matrix. The alloy exhibited excellent electrochemical corrosion resistance compare with 0Cr18Ni9 stainless steel in 1 mol/L HCl and 1 mol/L H<sub>2</sub>SO<sub>4</sub> solutions due to the formation of a stable and compact passive film (SiO<sub>x</sub>, MoO<sub>3</sub> and MoO<sub>2</sub>). Meanwhile, the chemical stability and strong bonds with large covalent component inherent to Mo<sub>5</sub>Si<sub>3</sub>-based alloy are also beneficial to its excellent corrosion resistance. However, the alloy displayed relatively low electrochemical corrosion resistance in 1 mol/L NaOH solution due to the formation and dissolution of Na<sub>2</sub>SiO<sub>3</sub> and damaging the integrity of SiO<sub>2</sub> preservative. Results of mass losses and surface morphologies indicate the excellent corrosion resistance of the Mo<sub>5</sub>Si<sub>3</sub>-based alloy during immersion in three test solutions. Only a slight pitting could be observed on the sample surface as a result of selective corrosion of the Mo<sub>3</sub>Si phases with respect to the Mo<sub>5</sub>Si<sub>3</sub> matrix after immersion for 100 h in NaOH solution.

#### ACKNOWLEDGMENTS

This research was supported by the Dr. Scientific Research Foundation of Liaocheng University (Grant No. 31805), Natural Science Foundation of Shandong Province (Grant No. ZR2011EL002). The authors acknowledge Mr Jiangang Jia and Ms Qiuxiang Song for their assistance on experiments of hot press sintering and electrochemical tests.

#### References

1. J.G. Gonzalez-Rodriguez, I. Rosales, M. Casales, S. Serna, L. Martinez, *Mater. Sci. Eng. A*. 371 (2004) 217
2. H.M. Wang, G. Duan, *Intermetallics*. 11 (2003) 755
3. S. Tao, D.Y. Li, *Wear*. 263 (2007) 363
4. Yanqiu Xia, Junhong Hu, Feng Zhou, Yimin Lin, Yulin Qiao, Tao Xu, *Mater. Sci. Eng. A*. 402 (2005) 135
5. Shizhong Wei, Jinhua Zhu, Leujue Xu, *Mater. Sci. Eng. A*. 404 (2005) 138
6. L. Yuan, H.M. Wang, *Electrochem Acta*. 54 (2008) 421
7. F. Neppel, G. Menzel, U. Schwabe, *J. Electrochem. Soc.* 130 (1983) 1174
8. M. Herranen, A. Delblanc Bauer, J.O. Carlsson, R.F., *Surf. Coat. Tech.* 96 (1997) 245
9. K Yoshimi, S. Nakatani, N. Nomura, S. Hanada, *Intermetallics*. 11 (2003) 787
10. C.L. Yeh, W.H. Chen, *J. Alloys Compd.* 438 (2007) 165
11. Jiang Xu, Chenghou Zhou, Shuyun Jiang, *Intermetallics*. 18 (2010) 1669
12. Erik Strom, Sten Eriksson, Hakan Rundlof, Ji Zhang, *Acta Mater.* 53 (2005) 357
13. Sergey A. Kuznetsov, Evgeny V. Rebrov, Martijn J.M. Mies, Mart H.J.M. de Croon, Jaap C. Schouten, *Surf. Coat. Tech.* 201 (2006) 971
14. Sharma Paswan, R. Mitra, S.K. Roy, *Mater. Sci. Eng. A*. 424 (2006) 251
15. R. Sakidja, J.S. Park, J. Hamann, J.H. Perepezko, *Scripta Mater.* 53 (2005) 723
16. J.G. Gonzalez-Rodriguez, I. Rosales, M. Casales, S. Serna, L. Martinez, *J. Solid State Electr.* 9 (2005) 691
17. L. Yuan, H.M. Wang, *Intermetallics*. 16 (2008) 1149
18. J.H. Yan, H.A. Zhang, S.W. Tang, J.G. Xu, *Mater Charact.* 60 (2009) 447
19. Q.D. Hu, P. Luo, Y.W. Yan, *J. Alloys Compd.* 468 (2009) 136
20. H.A. Zhang, X.Y. Liu, *Int J Refract Met H.* 19 (2001) 203
21. P.V. Krakhmalev, *Int J Refract Met H.* 22 (2004) 205
22. A. Kocijan, C. Donik, M. Jenko. *Corr. Sci.* 49(2007) 2083
23. G. Bianchi, A. Cerquetti, F. Mazza, S. Torchio, *Corr. Sci.* 12(1972) 495